

Programmable atom-photon quantum interface

Christoph Kurz, Pascal Eich, Michael Schug, Philipp Müller, and Jürgen Eschner*
Universität des Saarlandes, Experimentalphysik, Campus E2 6, 66123 Saarbrücken, Germany

We present the implementation of a programmable atom-photon quantum interface, employing a single trapped $^{40}\text{Ca}^+$ ion and single photons. Depending on its mode of operation, the interface serves as a bi-directional atom-photon quantum-state converter, as a source of entangled atom-photon states, or as a quantum frequency converter of single photons. The interface lends itself particularly to interfacing ions with SPDC-based single-photon or entangled-photon-pair sources.

PACS numbers: 03.67.Hk, 42.50.Ex, 42.50.Dv, 42.50.Ct

Quantum networks [1] integrate quantum-information processing and storage devices with quantum communication channels, allowing one to distribute quantum information between stationary network nodes through flying quantum bits (qubits). A platform that has proven suitable for this purpose is the combination of single trapped ions and single photons: while single ions allow for storing and processing quantum information [2–4], single photons are the only viable carriers of quantum information over long distance [5, 6]. In order to interconvert stationary and flying qubits, quantum interfaces are needed. Different approaches for the experimental implementation of atom-photon quantum interfaces have emerged. These include objectives and lenses of high numerical aperture [7, 8], deep parabolic mirrors [9, 10], and optical resonators [11–14]. With these systems, a number of essential quantum-networking building blocks have been realized, such as atom-photon entanglement [15, 16], atom-to-photon quantum-state mapping [17–19], heralded atom-atom entanglement [20, 21], quantum teleportation [22] and direct quantum-state transfer [23]. We demonstrated further basic prerequisites of a quantum network such as the high-rate generation of single photons in a pure quantum state [24] and the direct photonic interaction between distant single ions [25]. Recently, we implemented a protocol for high-fidelity heralded transfer of a photonic polarization qubit onto the qubit state of a single ion [26]. Here we report on a significant and comprehensive extension of that protocol, the realization of a programmable, bi-directional interface between a single ion and single photons, which depending on its mode of operation permits atom-to-photon or photon-to-atom quantum-state transfer, as well as generation of atom-photon entanglement; moreover, it is also suitable for quantum frequency conversion of single photons. Thereby the interface covers the essential operations required in quantum networks and especially for a quantum repeater [27].

Interface principle

Fig. 1 illustrates the general principle of the interface, experimentally implemented with the ground and excited states of a single $^{40}\text{Ca}^+$ ion. We first create a coherent superposition of the two outer Zeeman sublevels of the metastable $D_{5/2}$ state,

$$|\psi_D\rangle = \cos \frac{\vartheta_D}{2} |D, -\frac{5}{2}\rangle + \sin \frac{\vartheta_D}{2} e^{i\varphi_D} |D, +\frac{5}{2}\rangle, \quad (1)$$

and expose the ion to resonant photons on the $D_{5/2}$ to $P_{3/2}$ transition at 854 nm which are in a polarization state in the circular (R/L) basis,

$$|\psi_{854}\rangle = \cos \frac{\vartheta_{854}}{2} |854, R\rangle + \sin \frac{\vartheta_{854}}{2} e^{i\varphi_{854}} |854, L\rangle, \quad (2)$$

such that the input state of the interface is $|\Psi_{\text{in}}\rangle = |\psi_D\rangle |\psi_{854}\rangle$. Right-handed (R) and left-handed (L) circularly polarized 854 nm photons may be absorbed on the σ^+ and σ^- transition, respectively. Absorption of a photon triggers the emission of a single Raman photon on the $P_{3/2}$ to $S_{1/2}$ transition at 393 nm and transfers the ion to the $S_{1/2}$ ground state. For detection along the quantization axis, the two possible transitions, σ^+ and σ^- , translate to R- and L-polarized 393 nm photons, respectively. We hence obtain the ion-photon output state

$$|\Psi_{\text{out}}\rangle = \cos \frac{\theta}{2} |S, -\frac{1}{2}\rangle |393, L\rangle + \sin \frac{\theta}{2} e^{i\phi} |S, +\frac{1}{2}\rangle |393, R\rangle. \quad (3)$$

The evolution of the system from $|\Psi_{\text{in}}\rangle$ into the entangled state $|\Psi_{\text{out}}\rangle$ is described by [28]

$$|\Psi_{\text{out}}\rangle = (|S, -\frac{1}{2}\rangle |393, L\rangle \langle D, -\frac{5}{2}| \langle 854, R| + |S, +\frac{1}{2}\rangle |393, R\rangle \langle D, +\frac{5}{2}| \langle 854, L|) \cdot |\Psi_{\text{in}}\rangle$$

and used to realize the different interface operations: (i) when $|\psi_D\rangle$ and $|\psi_{854}\rangle$ are fixed, entangled atom-photon pairs are created (entangler operation); (ii) when $|\Psi_{\text{out}}\rangle$ is projected by detecting the 393 nm photon in a linear basis, the polarization state of the absorbed 854 nm photon is mapped into an atomic qubit state in $S_{1/2}$ (receiver operation); (iii) when the final atomic state is projected on a superposition of the Zeeman sublevels, the initial

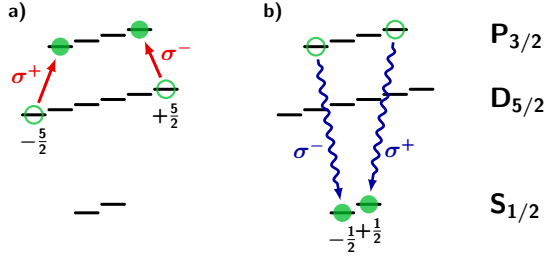


FIG. 1. General experimental scheme. Black bars denote the Zeeman sublevels of the involved atomic states $S_{1/2}$, $D_{5/2}$, and $P_{3/2}$. (a) Input state: the ion is coherently prepared in a superposition of the $|\pm \frac{5}{2}\rangle$ Zeeman sublevels of $D_{5/2}$ (filled green circles), and a photon at 854 nm in a superposition of the two circular polarizations is absorbed (red arrows). (b) Output state: a single 393 nm photon in a superposition of the two circular polarizations is emitted (blue arrows), leaving the ion in the corresponding superposition of the $|\pm \frac{1}{2}\rangle$ Zeeman sublevels of $S_{1/2}$ (filled green circles).

atomic state $|\psi_D\rangle$ is mapped into the polarization qubit of the output 393 nm photon (sender operation); (iv) finally, when both atomic superpositions are fixed, any input photon will be converted into a frequency-converted output photon of the corresponding polarization (converter operation). Receiver operation has been shown in [26], entangler and sender operation are demonstrated below. Quantum frequency conversion of photons from 854 nm to 393 nm is implicitly realized by these demonstrations.

Experimental procedure

Our experimental set-up is sketched in Fig. 2. A single $^{40}\text{Ca}^+$ ion is confined in a linear Paul trap and Doppler cooled by frequency-stabilized diode lasers [29]. A static magnetic field $B = 2.8 \text{ G}$ defines the quantization axis. Atomic state preparation in $|\psi_D\rangle$ is performed in three steps [26, 28]: first the ion is optically pumped to the $|- \frac{1}{2}\rangle$ level of $S_{1/2}$, then a radio-frequency (RF) $\pi/2$ -pulse from a coil below the trap excites the magnetic-dipole transition between the $S_{1/2}$ sublevels to form an equal superposition of $|\pm \frac{1}{2}\rangle$, and finally two π -pulses from a narrow-band laser at 729 nm coherently excite the $|\pm \frac{1}{2}\rangle$ populations to the respective $|\pm \frac{5}{2}\rangle$ levels in $D_{5/2}$.

A laser at 854 nm provides the polarized photons at 854 nm. Since for ion-to-photon state transfer as well as for ion-photon entanglement (sender and entangler operation) the 854 nm polarization is kept fixed, the laser propagation and polarization direction are both chosen orthogonal to the quantization axis. Photons at 393 nm emitted by the ion are collected along the quantization axis through an in-vacuum high-NA laser objective (HALO, [30]). The photons are projected onto a chosen polarization and sent to photomultiplier tubes (PMTs)

via multi-mode optical fibers. The output pulses of the PMTs, corresponding to the arrivals of single photons, are time-tagged for later processing. Another HALO collects fluorescence from cooling laser excitation.

Analysis of the final $S_{1/2}$ atomic state in the $|\pm \frac{1}{2}\rangle$ basis is performed by shelving the $|+\frac{1}{2}\rangle$ population in a sub-level of $D_{5/2}$ and illuminating the ion with the cooling light, which either reveals fluorescence (ion in $|- \frac{1}{2}\rangle$) or not (ion in $|+\frac{1}{2}\rangle$). For measuring in a superposition basis, an RF $\pi/2$ -pulse with the respective phase effects a basis rotation before shelving.

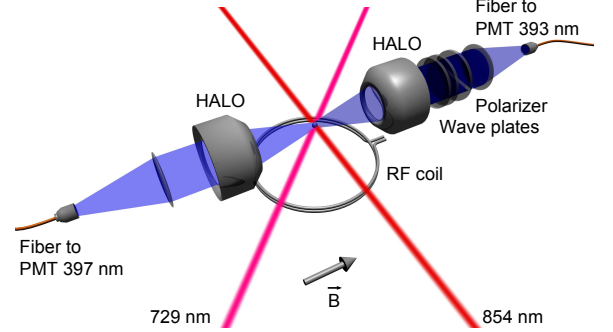


FIG. 2. Experimental set-up. HALO: high-NA laser objective, PMT: photomultiplier tube, Wave plates: one half-wave and one quarter-wave plate, \vec{B} : magnetic-field direction. The ion is trapped between the HALOs.

A typical experiment starts with the preparation of a given symmetric superposition in $D_{5/2}$ according to Eq. (1), which has angles $\vartheta_D = \frac{\pi}{2}$, and $\varphi_D = \varphi_{729} + \omega_L t$. Here φ_{729} is the (adjustable [28]) phase between the two preparation pulses of the 729 nm laser, and $\omega_L t$ is the phase that the superposition accumulates with time due to its Larmor precession [26, 28], $t = 0$ marking its preparation. The ion is excited with 854 nm photons of fixed linear polarization ($\vartheta_{854} = \frac{\pi}{2}$, $\varphi_{854} = \pi$), and detection events of 393 nm photons in various polarization bases are recorded in the form of arrival-time histograms. For verifying ion-to-photon state transfer as well as ion-photon entanglement, the correlation of these photon detections with the projection of the atom onto a specific superposition state is analyzed. Detection of the 393 nm photons with high time resolution ($\lesssim 320 \text{ ps}$ in our case) is crucial, in order to remove the frequency distinguishability of the two Raman scattering paths [31].

A representative data set is shown in Fig. 3(a). In this case, the atomic state is projected onto the superposition $|+\rangle = \frac{1}{\sqrt{2}}(|-\frac{1}{2}\rangle + |+\frac{1}{2}\rangle)$, and horizontally (H) and vertically (V) polarized photons are detected. The observed oscillations in the arrival-time distribution $P(t)$ agree, up to a reduced visibility, with the behaviour expected from the model [28],

$$P_{V,H}(t) \propto 1 \pm \cos(\varphi_{729} + \omega_L t). \quad (4)$$

The oscillation period of about 64 ns corresponds to the Larmor precession with $T = \frac{h}{4\mu_B B}$ expected for our static magnetic field $B = 2.8$ G and taking into account the Landé factors of the $S_{1/2}$ and $D_{5/2}$ manifolds. The overall envelope of $P(t)$ displays the exponential decay (with the Raman scattering rate) of the probability for the atom to remain in $D_{5/2}$ while it is exposed to the 854 nm photons.

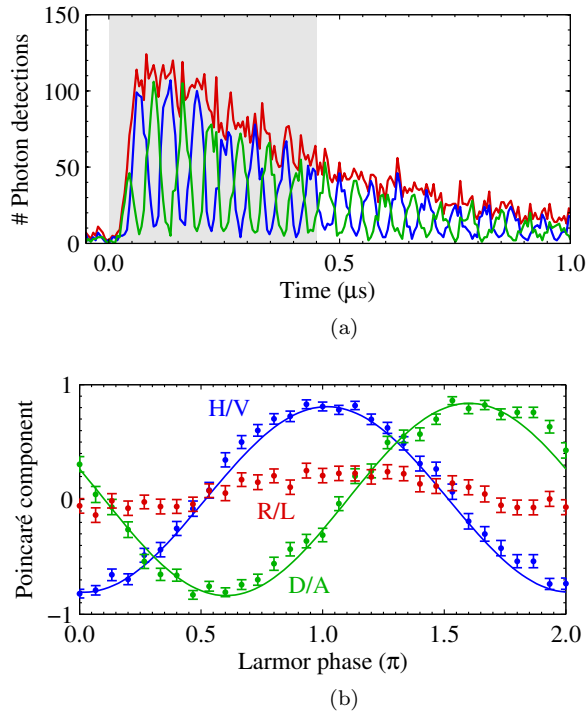


FIG. 3. Polarization analysis of single 393 nm photons. (a) Conditional photon arrival-time histograms, shown for photons projected onto the horizontal (blue) and vertical (green) polarization state, and conditioned on the projection of the ion onto the state $|+\rangle$. The red curve shows the unconditional arrival-time distribution, i.e. the sum of the blue and green histograms. The shaded area represents the time window used for data analysis. The bin size is 5 ns and the overall measuring time is 20 min. (b) State tomography of the photonic polarization for the same atomic-state preparation and projection as in (a). Shown are the three Poincaré components as functions of the Larmor phase. The solid lines are sinusoidal fits.

From data as in Fig. 3(a), we perform full tomography of the photonic polarization. We project the photon onto the three bases of linear (H/V and D/A) and circular (R/L) polarization by appropriate settings of the half-wave and quarter-wave plate. As a trade-off between high fidelity of the photonic state and high detection efficiency, we select detection events within the first 450 ns of the arrival-time distribution, and we display them as a function of the Larmor phase $\varphi_L = 2\pi(\frac{t}{T} \bmod 1)$. Fig. 3(b) shows the Poincaré components of the reconstructed polarization state. As expected, the linear polarization rotates with the Larmor phase, and the two linear bases

show a $\frac{\pi}{2}$ phase difference. The ellipticity of the polarization (R/L component) is close to zero, with a slightly visible oscillation originating from a non-perfect calibration of the wave plates.

Entangler operation

In order to verify the operation of our interface as a source of entangled ion-photon states, we perform standard quantum-state tomography [32] of the two-qubit system through correlation measurements in the product bases of photonic and atomic qubit. Using a maximum-likelihood approach [32], we reconstruct the physical quantum state that is most likely to have produced the experimental data. From the derived density matrix, depicted in Fig. 4, we find a fidelity $F = 84.6(2)\%$ with respect to the maximally entangled state (Eq. (3)) for our 450 ns time window. This value exceeds the classical threshold of $\frac{2}{3}$ by more than 80 standard deviations and thus clearly indicates the creation of entanglement at the output of our interface.

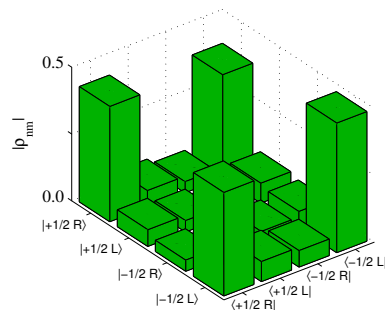


FIG. 4. Density matrix of the entangled ion-photon state in the product basis. Shown are the moduli of the matrix entries.

The two main sources of infidelity in our set-up are currently magnetic-field fluctuations which limit the atomic coherence time and, as mentioned above, non-perfectly calibrated wave plates. The photon-detection efficiency for this experiment amounts to 0.353(1)%, including that only 50% of the arriving photons are transmitted through the polarization analyzer. At 11 kHz repetition rate and taking the PMT quantum efficiency of 28(1)% into account, we obtain $140(5)\text{ s}^{-1}$ fiber-coupled photons that are entangled with the ion; removing the polarization analysis would double that rate.

Sender operation

Operation of our interface for ion-to-photon quantum-state transfer is accomplished when a prepared atomic input state, characterized by angles ϑ_D and φ_D (Eq. 1) leads to the emission of a 393 nm output photon in the

corresponding polarization state. This interface operation involves projection of the final atomic state onto a fixed superposition, for which we choose the $|+\rangle$ state. In this case the 393 nm photon detected at time t will be described by

$$|\psi_{393}\rangle = \cos\frac{\theta}{2}|R\rangle - \sin\frac{\theta}{2}e^{i\phi}|L\rangle \quad (5)$$

with $\theta = \vartheta_D$ and $\phi = \varphi_{729} + \omega_L t$. One sees that the Larmor precession of the input state enters into the polarization of the output state. This is convenient for verification of the interface (see below); it has to be taken into account as a time-dependent phase shift when the interface is operated in a quantum communication scenario.

First, we prepare the four symmetric ($\vartheta_D = \frac{\pi}{2}$) superposition states with $\varphi_{729} = \{0, \frac{\pi}{2}, \pi, \frac{3\pi}{2}\}$ and analyze the photonic phase, i.e., the direction of the linear polarization of the 393 nm photon. The result is displayed in Fig. 5(a): the linear dependence with steps of $\frac{\pi}{2}$ between the four lines shows that the photonic phase reflects faithfully both the Larmor phase $\omega_L t$ and φ_{729} .

In a second step, we perform full quantum-process tomography of the atom-to-photon state mapping process by using also the bare input states $|\pm\frac{5}{2}\rangle$ and analyzing the photonic state in all three polarization bases. This allows us to reconstruct the process matrix χ , defined through $\rho_{\text{out}} = \sum_{m,n} \chi_{mn} \sigma_m \rho_{\text{in}} \sigma_n$ with the Pauli matrices $\{\sigma_{i=1,\dots,4}\} = \{\mathbb{1}, \sigma_x, \sigma_y, \sigma_z\}$ [33]. The matrix is displayed in Fig. 5(b). The value χ_{11} represents the identity part of the quantum process and is known as the process fidelity. From our experimental data, we derive $\chi_{11} = 90.2(1.0)\%$. Another measure for the quality of the state transfer is the mean fidelity of the reconstructed photonic states with respect to the atomic input states; averaged over all six input states, it amounts to $92.4(3)\%$. It is instructive to investigate how the two figures of merit behave as a function of the detection time window, which is depicted in Fig. 5(c); the same figure shows the trade-off between fidelity and success probability of the interface. For the 450 ns time window, we achieve $0.127(1)\%$ mean photon detection efficiency. At 10 kHz repetition rate, we obtain $45(2)\text{ s}^{-1}$ fiber-coupled photons. The efficiency reduction compared to the previous measurement is caused by using different wave plates that are better calibrated but have smaller aperture. Removing the wave plates and polarizer would allow us to transfer the atomic qubit state onto fiber-coupled photons at an estimated rate of $\sim 300\text{ s}^{-1}$, similar to that for ion-photon entanglement.

An important source of infidelity for both ion-photon entanglement and ion-to-photon quantum-state transfer are magnetic-field fluctuations in the vicinity of the trap apparatus that limit the coherence of the atomic qubit state. We expect to mitigate this issue by means of an active magnetic-field stabilization. Additional minor

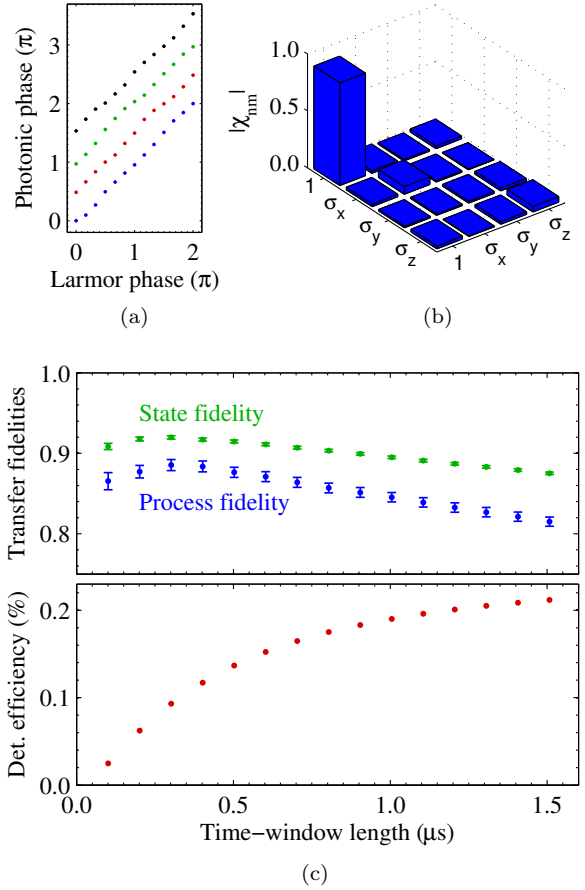


FIG. 5. Characterization of ion-to-photon quantum-state transfer. (a) Phase of the photon's linear polarization as a function of the Larmor phase and for $\varphi_{729} = \{0, \frac{\pi}{2}, \pi, \frac{3\pi}{2}\}$ (top to bottom). (b) Quantum-process matrix in the Pauli basis. Shown are the moduli of the matrix entries. (c) Process fidelity (blue dots), mean quantum-state fidelity (green dots) and detection efficiency for different lengths of the detection time window. Where not indicated, error bars are smaller than the size of the symbols.

sources of infidelity are detector dark counts ($\sim 30\text{ s}^{-1}$) and spontaneous decay from the $P_{3/2}$ state back to $D_{5/2}$ (with 5.87 % probability [34]).

Conclusions

In conclusion, we demonstrated a single-atom to single-photon quantum interface that is programmable to serve for bi-directional quantum-state transfer and generation of atom-photon entanglement, essential operations in quantum networks, especially for a quantum repeater. Entangled ion-photon pairs have been created at close to 300 s^{-1} rate (entangler operation). The reconstructed two-qubit state exhibits $84.6(2)\%$ fidelity with respect to a maximally entangled state. Using the same ingredients, we realized ion-to-photon quantum-state transfer (sender

operation): an arbitrary atomic qubit state is mapped onto the polarization state of the output photon with 90.2(1.0) % quantum-process fidelity and 92.4(3) % mean quantum-state fidelity. Application of the same interface for heralded photon-to-atom quantum-state transfer (receiver operation) had been shown earlier [26]. Finally, the converter mode of operation of the interface provides single-photon frequency conversion, with a single atom replacing the conventional non-linear optical device [35, 36]. Our experimental implementation is based on a Raman transition in a single $^{40}\text{Ca}^+$ ion and is readily adapted to other ions and neutral atoms such as Rb. Its versatility and simplicity makes the interface a valuable tool for quantum repeater and hybrid (see, e.g., [37]) quantum networking technology.

Acknowledgments. We gratefully acknowledge partial support by the BMBF (QuOREP project, QSCALE Chist-ERA project, Q.Com-Q project).

* juergen.eschner@physik.uni-saarland.de

- [1] H. J. Kimble. *The quantum internet*. Nature **453**, 1023–1030 (2008).
- [2] D. Leibfried, B. DeMarco, V. Meyer, D. Lucas, M. Barrett, J. Britton, W. M. Itano, B. Jelenković, C. Langer, T. Rosenband, D. J. Wineland. *Experimental demonstration of a robust, high-fidelity geometric two ion-qubit phase gate*. Nature **422**, 412–415 (2003).
- [3] C. Langer, R. Ozeri, J. D. Jost, J. Chiaverini, B. DeMarco, A. Ben-Kish, R. B. Blakestad, J. Britton, D. B. Hume, W. M. Itano, D. Leibfried, R. Reichle, T. Rosenband, T. Schaetz, P. O. Schmidt, D. J. Wineland. *Long-Lived Qubit Memory Using Atomic Ions*. Phys. Rev. Lett. **95**, 060502 (2005).
- [4] J. Benhelm, G. Kirchmair, C. F. Roos, R. Blatt. *Towards fault-tolerant quantum computing with trapped ions*. Nat. Phys. **4**, 463–466 (2008).
- [5] G. Weihs, T. Jennewein, C. Simon, H. Weinfurter, A. Zeilinger. *Violation of Bell’s Inequality under Strict Einstein Locality Conditions*. Phys. Rev. Lett. **81**, 5039 (1998).
- [6] X.-S. Ma, T. Herbst, T. Scheidl, D. Wang, S. Kropatschek, W. Naylor, B. Wittmann, A. Mech, J. Kofler, E. Anisimova, V. Makarov, T. Jennewein, R. Ursin, A. Zeilinger. *Quantum teleportation over 143 kilometres using active feed-forward*. Nature **489**, 269–273 (2012).
- [7] M. K. Tey, Z. Chen, S. A. Aljunid, B. Chng, F. Huber, G. Maslennikov, C. Kurtsiefer. *Strong interaction between light and a single trapped atom without the need for a cavity*. Nat. Phys. **4**, 924–927 (2008).
- [8] G. Vittorini, D. Hucul, I. V. Inlek, C. Crocker, C. Monroe. *Entanglement of distinguishable quantum memories*. Phys. Rev. A **90**, 040302(R) (2014).
- [9] R. Maiwald, D. Leibfried, J. Britton, J. C. Bergquist, G. Leuchs, D. J. Wineland. *Stylus ion trap for enhanced access and sensing*. Nat. Phys. **5**, 551–554 (2009).
- [10] M. Fischer, M. Bader, R. Maiwald, A. Golla, M. Sondermann, G. Leuchs. *Efficient saturation of an ion in free space*. Appl. Phys. B **117**, 797–801 (2014).
- [11] C. J. Hood, M. S. Chapman, T. W. Lynn, H. J. Kimble. *Real-Time Cavity QED with Single Atoms*. Phys. Rev. Lett. **80**, 4157–4160 (1998).
- [12] M. Hennrich, T. Legero, A. Kuhn, G. Rempe. *Vacuum-Stimulated Raman Scattering Based on Adiabatic Passage in a High-Finesse Optical Cavity*. Phys. Rev. Lett. **85**, 4872–4875 (2000).
- [13] A. B. Mundt, A. Kreuter, C. Becher, D. Leibfried, J. Eschner, F. Schmidt-Kaler, R. Blatt. *Coupling a Single Atomic Quantum Bit to a High Finesse Optical Cavity*. Phys. Rev. Lett. **89**, 103001 (2002).
- [14] M. Keller, B. Lange, K. Hayasaka, W. Lange, H. Walther. *Deterministic coupling of single ions to an optical cavity*. Appl. Phys. B **76**, 125–128 (2003).
- [15] B. B. Blinov, D. L. Moehring, L.-M. Duan, C. Monroe. *Observation of entanglement between a single trapped atom and a single photon*. Nature **428**, 153–157 (2004).
- [16] J. Volz, M. Weber, D. Schlenk, W. Rosenfeld, J. Vrana, K. Saucke, C. Kurtsiefer, H. Weinfurter. *Observation of Entanglement of a Single Photon with a Trapped Atom*. Phys. Rev. Lett. **96**, 030404 (2006).
- [17] A. D. Boozer, A. Boca, R. Miller, T. E. Northup, H. J. Kimble. *Reversible State Transfer between Light and a Single Trapped Atom*. Phys. Rev. Lett. **98**, 193601 (2007).
- [18] T. Wilk, S. C. Webster, A. Kuhn, G. Rempe. *Single-Atom Single-Photon Quantum Interface*. Science **317**, 488–490 (2007).
- [19] A. Stute, B. Casabone, B. Brandstätter, K. Friebe, T. E. Northup, R. Blatt. *Quantum-state transfer from an ion to a photon*. Nat. Photon. **7**, 219–222 (2013).
- [20] D. L. Moehring, P. Maunz, S. Olmschenk, K. C. Younge, D. N. Matsukevich, L.-M. Duan, C. Monroe. *Entanglement of single-atom quantum bits at a distance*. Nature **449**, 68–71 (2007).
- [21] J. Hofmann, M. Krug, N. Ortegel, L. Gérard, M. Weber, W. Rosenfeld, H. Weinfurter. *Heralded Entanglement Between Widely Separated Atoms*. Science **337**, 72–75 (2012).
- [22] S. Olmschenk, D. N. Matsukevich, P. Maunz, D. Hayes, L.-M. Duan, C. Monroe. *Quantum Teleportation Between Distant Matter Qubits*. Science **323**, 486–489 (2009).
- [23] C. Nölleke, A. Neuzner, A. Reiserer, C. Hahn, G. Rempe, S. Ritter. *Efficient Teleportation Between Remote Single-Atom Quantum Memories*. Phys. Rev. Lett. **110**, 140403 (2013).
- [24] C. Kurz, J. Huwer, M. Schug, P. Müller, J. Eschner. *A high-rate source for single photons in a pure quantum state*. New J. Phys. **15**, 055005 (2013).
- [25] M. Schug, J. Huwer, C. Kurz, P. Müller, J. Eschner. *Heralded Photonic Interaction between Distant Single Ions*. Phys. Rev. Lett. **110**, 213603 (2013).
- [26] C. Kurz, M. Schug, P. Eich, J. Huwer, P. Müller, J. Eschner. *Experimental protocol for high-fidelity heralded photon-to-atom quantum state transfer*. Nat. Commun. **5**, 5527 (2014).
- [27] H.-J. Briegel, W. Dür, J. I. Cirac, P. Zoller. *Quantum Repeaters: The Role of Imperfect Local Operations in Quantum Communication*. Phys. Rev. Lett. **81**, 5932 (1998).
- [28] M. Schug, C. Kurz, P. Eich, J. Huwer, P. Müller, J. Eschner. *Quantum interference in the absorption and emission of single photons by a single ion*. Phys. Rev. A **90**, 023829 (2014).

- [29] F. Rohde, M. Almendros, C. Schuck, J. Huwer, M. Hennrich, J. Eschner. *A diode laser stabilization scheme for $^{40}\text{Ca}^+$ single-ion spectroscopy*. J. Phys. B **43**, 115401 (2010).
- [30] S. Gerber, D. Rotter, M. Hennrich, R. Blatt, F. Rohde, C. Schuck, M. Almendros, R. Gehr, F. Dubin, J. Eschner. *Quantum interference from remotely trapped ions*. New J. Phys. **11**, 013032 (2009).
- [31] E. Togan, Y. Chu, A. S. Trifonov, L. Jiang, J. Maze, L. Childress, M. V. G. Dutt, A. S. Sorensen, P. R. Hemmer, A. S. Zibrov, M. D. Lukin. *Quantum entanglement between an optical photon and a solid-state spin qubit*. Nature (London) **466**, 730–734 (2010).
- [32] D. F. V. James, P. G. Kwiat, W. J. Munro, A. G. White. *Measurement of qubits*. Phys. Rev. A **64**, 052312 (2001).
- [33] I. L. Chuang, M. A. Nielsen. *Prescription for experimental determination of the dynamics of a quantum black box*. J. Mod. Opt. **44**, 2455–2467 (1997).
- [34] R. Gerritsma, G. Kirchmair, F. Zähringer, J. Benhelm, R. Blatt, C. F. Roos. *Precision measurement of the branching fractions of the $4p^2P_{3/2}$ decay of Ca II*. Eur. Phys. J. D **50**, 13–19 (2008).
- [35] R. Ikuta, Y. Kusaka, T. Kitano, H. Kato, T. Yamamoto, M. Koashi, N. Imoto. *Wide-band quantum interface for visible-to-telecommunication wavelength conversion*. Nat. Commun. **2**, 537 (2011).
- [36] S. Zaske, A. Lenhard, C. A. Keßler, J. Kettler, C. Hepp, C. Arend, R. Albrecht, W.-M. Schulz, M. Jetter, P. Michler, C. Becher. *Visible-to-Telecom Quantum Frequency Conversion of Light from a Single Quantum Emitter*. Phys. Rev. Lett. **109**, 147404 (2012).
- [37] H. M. Meyer, R. Stockill, M. Steiner, C. Le Gall, C. Matthiesen, E. Clarke, A. Ludwig, J. Reichel, M. Atatüre, M. Köhl. *Direct Photonic Coupling of a Semiconductor Quantum Dot and a Trapped Ion*. Phys. Rev. Lett. **114**, 123001 (2015).